Ultrafast Nonlinear Optical Response of Two-dimensional MoS_2/Bi_2Te_3 Heterostructure①

DONG Jun-Hao[a, d] PAN Jia[c] YE Chen-Yu[b]
WANG Ru[b] HUANG Yong-Feng[b] ZHENG Jing-Ying[b]
ZHAN Hong-Bing[b②] WANG Qian-Ting[a, d②]

[a] (*School of Materials Science and Engineering, Fujian University of Technology, Fuzhou* 350118, *China*)

[b] (*College of Materials Science and Engineering, Fuzhou University, Fuzhou* 350108, *China*)

[c] (*School of Electronic, Electrical Engineering and Physics, Fujian University of Technology, Fuzhou* 350118, *China*)

[d] (*Fujian Provincial Key Laboratory of Advanced Materials Processing and Application, Fuzhou* 350118, *China*)

ABSTRACT Controlled stacking of different two-dimensional (2*D*) atomic layers hold great promise for significantly optimizing the optical properties of 2*D* materials and broadening their applications. Here, vertical 2*D* MoS_2/Bi_2Te_3 heterostructures with high crystallinity and optical quality have been successfully constructed, through drop-casting 2*D* Bi_2Te_3 flakes on chemical vapor deposition (CVD)-grown MoS_2 flakes. Based on our homebuilt micro *Z*-scan and pump-probe measurement, we precisely investigated and compared the nonlinear optical (NLO) performance of an individual micro-sized MoS_2 flake before and after stacking 2*D* Bi_2Te_3 nanoplates. Moreover, layer-dependent ultrafast carrier dynamics of CVD-grown MoS_2 flakes were also explored. Owing to the efficient charge transfer from the monolayer (1 L) MoS_2 to 2*D* Bi_2Te_3, the 1L MoS_2/Bi_2Te_3 heterostructure demonstrated excellent NLO performance with superior nonlinear saturable absorption coefficient and ultrashort carrier lifetime. Our work greatly enriches our understanding of 2*D* heterostructure and paves the way for designing new type of tunable 2*D* photonics materials by combining the optical advantages of different 2*D* materials.

Keywords: two-dimensional materials, nonlinear optics, ultrafast response;

DOI: 10.14102/j.cnki.0254-5861.2011-3183

1 INTRODUCTION

The two-dimensional (2*D*) layered materials have attracted considerable attention due to their diverse and potentially useful electronic and optical properties such as nonlinear optical (NLO) properties[1, 2]. Among these emerging materials, 2*D* MoS_2 as the representative one owns the layered-dependent electronic structure evolution from an indirect band gap of 1.3 eV for the bulk to a direct gap of 1.9 eV for a monolayer[3, 4]. Their atomic thickness together with peculiar electronic structure has endowed them with excellent optical properties such as strong saturable NLO absorption and moderate modulation depth[5-7], which enabled their promising varied applications in optical switches, Q-switching and mode locking pulse lasers and other photonic devices[8-10]. In addition, these optical properties of 2*D* MoS_2 could be specified by the dynamics of free carriers and bound excitons, providing a novel platform to investigate involved fascinating physical mechanisms[11, 12]. Unfortunately, limited NLO response time obtained by the analysis of ultrafast carrier dynamics makes them uncompetitive in the devices based on ultrashort laser pulse generation[13, 14]. Unlike typical semiconductor MoS_2, Bi_2Te_3 as a topological insulator possesses a narrow bandgap (~0.3 eV) bulk state and the Dirac-like linear dispersion band on the surface states[15]. As a result, they exhibit broadband saturable NLO absorption and ultrafast carrier cooling rate, suitable for building ultrafast optical devices operated at ultrabroad wavelength[10, 16, 17].

Received 18 March 2021; accepted 19 April 2021

① This research was supported by the Central Government Research Programs to Guide the Local Scientific and Technological Development (No. 2018L3001), National Natural Science Foundation of China (No. 51872048, U1732155) and Natural Science Foundation of Fujian Province (No. 2020J01353)

② Corresponding author. E-mail: hbzhan@fzu.edu.cn and wqt@fjut.edu.cn

Nevertheless, this unique electronic structure also leads to their weak NLO absorption intensity and low modulation depth, hindering the stable mode-locking operation for ultrafast pulse laser[18-20].

Compared to individual counterparts, vertically stacking different layers with distinct band structures to form layered heterostructures with van der Waals (vdW) interaction offers a promising approach for optimized performance engineering[21, 22]. Unique electronic properties of each individual layer might not be greatly perturbed by the interlayer weak vdW interaction, and the difference in work functions and the interfacial photophysics processes between different layers may enable the generated vertical heterostructures to exhibit tunable properties and novel physical phenomena. For instance, vertical MoS_2/WS_2, MoS_2/ReS_2, and MoS_2/graphene heterostructures showed great potentials in future optoelectronic applications owing to the fast charge transfer in their interfaces and diverse excitation and relaxation routes of photoexcited quasiparticles[23-26]. Therefore, inspired by the great availability of heterostructure and the unique performance of MoS_2 and Bi_2Te_3, it is exciting to combine Bi_2Te_3 with MoS_2 and thus construct vertical MoS_2/Bi_2Te_3 heterostructures for further investigating their functional properties. Recently, significant photoluminescence quenching with fast charge transfer and ultrafast hot-carrier photovoltaic devices have been demonstrated in MoS_2/Bi_2Te_3 heterostructures[27, 28]. However, relevant researches on 2*D* MoS_2/Bi_2Te_3 heterostructure and their nonlinear optical properties are quite limited.

Here, we prepared vertical MoS_2/Bi_2Te_3 heterostructures by stacking 2*D* Bi_2Te_3 nanoplates on chemical vapor deposition (CVD)-grown MoS_2 flakes. The high crystallinity and optical quality of the obtained MoS_2/Bi_2Te_3 heterostructures were confirmed by transmission electron microscope (TEM), Raman and ultraviolet-visible (UV-Vis) absorption spectroscopies. Especially, we built *Z*-scan measurements with micro optical imaging and accurately determined the much higher nonlinear saturable absorption coefficient of (-1.3×10^4)~(-2.2×10^4) cm/GW in MoS_2/Bi_2Te_3 heterostructures than those of 2*D* Bi_2Te_3 flakes $((-7.0\times10^3)$~(-9.0×10^3) cm/GW). Additionally, ultrafast carrier dynamics following femtosecond laser 400 nm excitation were utilized to unravel more detailed photophysical process accounting for the NLO response in these samples. The CVD-grown monolayer (1L) MoS_2 flakes demonstrated the fastest carrier lifetime (~620 fs) than 2L, 3L and 4L counterparts, and provided an ideal material for the construction of 1L MoS_2/Bi_2Te_3 heterostructure. Expectedly, shorter carrier lifetime of ~440 fs was obtained on 1L MoS_2/Bi_2Te_3 heterostructures due to the charge transfer from the 1L MoS_2 to 2*D* Bi_2Te_3.

2 EXPERIMENTAL

2. 1 Preparation of the MoS_2, Bi_2Te_3 and MoS_2/Bi_2Te_3 heterostructures

Our 2*D* MoS_2 flakes with varied layer numbers were obtained by CVD according to the previously reported method[29]. More specifically, the sulfur powders and electrochemical oxidized Mo foils as precursors were utilized to synthesize MoS_2. The electrochemical anodization of Mo foils (Alfa-Aesar, 0.025 mm) was performed at a current of 0.04 A for 10 minutes at room temperature. After that, oxidized Mo foils were arched on double-sided polished Al_2O_3 substrates at the center of the furnace. Sulfur powders (Alfa-Aesar, 99.999%, 1.5 g) were placed in the upstream and heated by heating belt at 190 ℃ when the temperature of the furnace reached 630 ℃. Then, the furnace was heated to 880 ℃ for 10 minutes and naturally cooled. To synthesize Bi_2Te_3 flakes, the solvothermal method was carried out[17, 30]. 0.64 g polyvinylpyrrolidone (Aladdin, AR) was dissolved in 20 mL ethylene glycol to form a clear solution, followed by the addition of 0.221 g $BiCl_3$ (Aladdin, 99.99%), 0.21 g Na_2TeO_3 (Aladdin, 99.99%) and 0.56 g NaOH (Aladdin, AR). Next, the resulting precursor suspension was stirred for 1 h and then sealed in the autoclave (50 mL). Afterwards, the autoclave was heated to 180 ℃ for 6 h, followed by cooling to room temperature naturally. The obtained solution was centrifuged at 8500 r/min. Then, the obtained solid product was washed with deionized water and ethylene glycol, and finally dispersed in ethylene glycol. To construct MoS_2/Bi_2Te_3 heterostructures, 1 mL Bi_2Te_3 solution was dropped on the substrate with as-grown MoS_2 flakes. Additionally, the produced MoS_2/Bi_2Te_3 heterostructures were annealed at 200 ℃ in pure Ar atmosphere to enhance the coupling between the layers.

2. 2 Characterizations

Optical images were captured with Olympus BX 53M microscope. Atomic force microscope (AFM) images were carried out with Bruker Dimension Icon. TEM experiment was performed with the Tecnai Talos F200i. Raman measurements were taken with Horiba-Jobin-Yvon Raman

system at 532 nm laser, and the Si peak at 520.7 cm^{-1} was used for calibration in the data analysis.

The open aperture *Z*-scan and pump-probe techniques were employed with the homebuilt equipments. A diode-pump Yb medium femtosecond laser system with pulse repetition rate of 100 kHz, a center wavelength at 1030 nm, and a pulse width of ~190 fs was used as the excitation source. And an optical parametric amplifier (OPA) was also equipped to tune the varied wavelengths from 400 to 1500 nm. For *Z*-scan measurements, the wavelength of photoexcitation source was fixed on 400 nm. The samples on the double-sided polished Al_2O_3 substrates with ~0.5 mm thickness were mounted on a linear translation stage which could move near the focus to imitate the change of the laser intensity. Especially, the objective lens and camera were introduced in this system to observe and identify the samples as illustrated in Fig. 3a. Then, the spot of laser source was also focused on the targeted samples to realize micro-*Z*-scan characterization. For pump-probe measurements, the 400 nm laser was used to excite photocarriers in the samples and the OPA was utilized to generate probe beams with the wavelengths from 400 to 800 nm.

3 RESULTS AND DISCUSSION

3. 1 Structure characterization and spectroscopic properties of the obtained MoS_2/Bi_2Te_3 heterostructures

The vertical MoS_2/Bi_2Te_3 heterostructure was schematically illustrated in Fig. 1a. The bottom CVD-grown MoS_2 monolayers exhibited the length in the range of ~30~50 μm confirmed by optical and AFM images (Figs. 1b and 1c and Supplementary materials, Fig. S1), which was suitable for surviving reliable micro-optical measurements involving following *Z*-scan and ultrafast transient absorption spectroscopy. For upper stacked Bi_2Te_3 flakes, the size and thickness were about 500~600 nm and 15~20 nm, respectively. And these Bi_2Te_3 flakes were dispersedly on 1L MoS_2 flakes with high coverage to form MoS_2/Bi_2Te_3 heterostructures. To further evaluate the crystallinity and structures of the as-prepared samples, we transferred the targeted samples to the holey carbon grids for TEM characterizations[31]. TEM images captured on MoS_2/Bi_2Te_3 heterostructures showed triangular MoS_2 and hexagonal Bi_2Te_3 flakes (Fig. 1d), consistent with the AFM measurements. For the high resolution TEM (HRTEM) images, 2*D* MoS_2 and Bi_2Te_3 flakes demonstrated unambiguous lattice stripes with lattice spacing of 0.27 and 0.22 nm, assigned to their (100) and (110) planes, respectively (see the insets of Fig. 1d). All selected-area electron diffraction (SAED) patterns taken at varied regions of the pure MoS_2 monolayer exhibited only one set of hexagonally arranged diffraction spots, confirming its single crystalline nature over a large area (Fig. 1d and Supplementary materials, Fig. S2a). And the Bi_2Te_3 flake also displayed SAED patterns of only one hexagonally diffraction spot (Fig. 1d and Supplementary materials, Figs. S2b and 2c), indicating its good crystallinity. Combined both of them, the MoS_2/Bi_2Te_3 heterostructure shows two sets of clear hexagonal diffraction spots (Fig. 1d), indicating its high quality and undamaged preparation process.

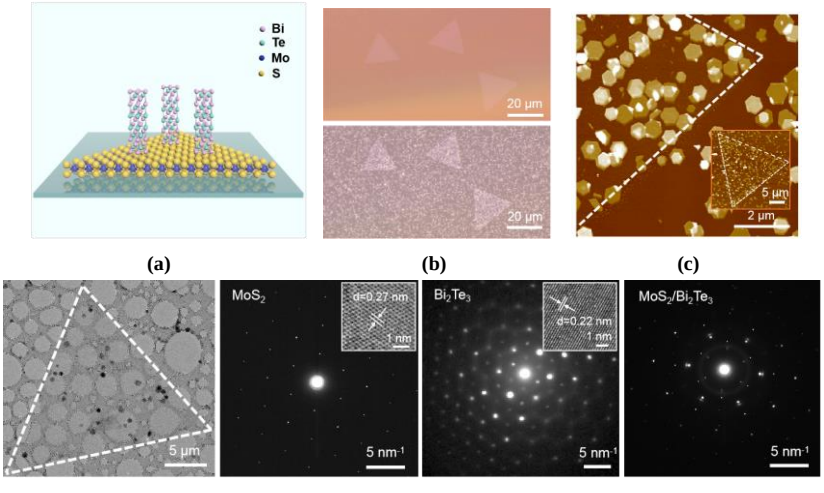

Fig. 1. (a) Schematic of vertical MoS_2/Bi_2Te_3 heterostructure, (b) Optical images taken from monolayer MoS_2 flakes (upper) and their corresponding MoS_2/Bi_2Te_3 heterostructures, (c) Enlarged AFM image of a MoS_2/Bi_2Te_3 heterostructure. Inset: AFM image of the complete triangle MoS_2/Bi_2Te_3 heterostructure, (d) TEM image of a MoS_2/Bi_2Te_3 heterostructure, SAED patterns of the MoS_2, Bi_2Te_3 and MoS_2/Bi_2Te_3 heterostructure from left to right, respectively. Insets: the corresponding HRTEM images of MoS_2 and Bi_2Te_3

Next, the spectroscopic properties of MoS_2/Bi_2Te_3 heterostructures were investigated. We first conducted Raman spectra on these flakes and found five observable peaks as shown in Fig. 2a. The prominent diffraction peaks at ~60, ~101 and ~134 cm^{-1} were indexed to the out-of-plane $A_{1g}{}^1$, the in-plane $E_g{}^2$ and the out-of-plane $A_{1g}{}^2$ vibration modes of 2*D* Bi_2Te_3, respectively[32, 33]. Two characteristic peaks at ~382 and ~403 cm^{-1} were associated with the in-plane $E_{2g}{}^1$ and out-of-plane A_{1g} vibration modes of 1L MoS_2, respectively[34, 35]. The co-existence of the feature peaks of these two flakes further confirmed the successful preparation of high-quality MoS_2/Bi_2Te_3 heterostructures. Then, UV-vis absorbance spectra were utilized to study the linear optical response of MoS_2, Bi_2Te_3 and MoS_2/Bi_2Te_3 heterostructures (Fig. 2b). The 2*D* Bi_2Te_3 flakes showed broad optical absorbance at 400~800 nm. Two characteristic peaks of ~623 and ~671 nm anticipated for 1L MoS_2 flakes were observed, assigned to its B (~2.0 eV) and A (~1.9 eV) excitonic transition[5, 36]. The absorbance of MoS_2/Bi_2Te_3 heterostructure was higher than that of MoS_2 and Bi_2Te_3 only, suggesting their enhancement of the linear absorption.

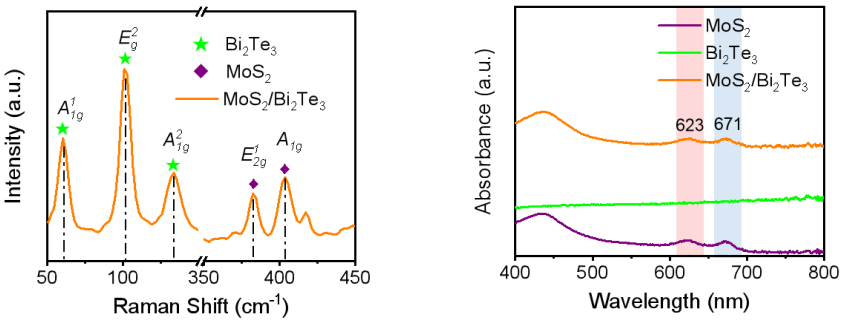

(a) **(b)**

Fig. 2. (a) Raman spectrum of a MoS_2/Bi_2Te_3 heterostructure, (b) UV-Vis spectra of MoS_2 flakes (purple), Bi_2Te_3 flakes (green) and MoS_2/Bi_2Te_3 heterostructures (orange)

3. 2 Nonlinear optical properties of the obtained MoS_2/Bi_2Te_3 heterostructures

To more precisely investigate the nonlinear absorption properties of as-prepared 2*D* MoS_2, Bi_2Te_3 and MoS_2/Bi_2Te_3 heterostructures, we designed a homemade micro-*Z*-scan technique equipped with a microscopic imaging system as shown in Fig. 3a. In this system, optical microscope and camera were introduced to observe and locate the samples, which greatly facilitated the focus and irradiation of following photoexcitation on the targeted samples to realize micro-*Z*-scan characterization (Fig. 3b). Therefore, we could accurately compare the NLO properties of the same MoS_2 flake before and after constructing with 2*D* Bi_2Te_3. Figs. 3c and 3e showed the typical *Z*-scan curves of as-made 1L MoS_2, 2*D* Bi_2Te_3 and MoS_2/Bi_2Te_3 heterostructures under the excited laser pulse of 400 nm (3.1 eV) with ~190 fs pulse width, respectively. We found that these MoS_2, Bi_2Te_3 and MoS_2/Bi_2Te_3 heterostructures all exhibited obvious saturation absorption and the transmittance intensity gradually increased with the increase of incident excitation energy. In addition, compared with pure 2*D* MoS_2 and Bi_2Te_3, the MoS_2/Bi_2Te_3 heterostructures demonstrated larger transmittance and thus saturable intensity under the same input intensity toward the focus (Fig. 3f), indicating their enhanced light-matter interaction[37]. This enhancement probably originated from the electron transfer from 1L MoS_2 to 2*D* Bi_2Te_3 flakes after photoexcitation due to the higher Fermi energy of MoS_2 than Bi_2Te_3[38, 39].

Furthermore, the nonlinear absorption coefficient (β) was adopted to quantitatively describe the NLO properties of these materials. The *Z*-scan results can be fitted by equation (1) according to a nonlinear absorption model[38, 40]:

$$T = \sum_{m-0}^{\infty} \frac{\left[-\beta I_0 L_{eff} / \left(1+z^2/z_0^2\right)\right]^m}{(m+1)^{3/2}} \approx 1 - \frac{\beta I_0 L_{eff}}{2\sqrt{2}\left(1+z^2/z_0^2\right)} \quad (1)$$

where $L_{\text{eff}} = \left(1-e^{-\alpha_0 L}\right)/\alpha_0$ is the effective length of the sample; L and α_0 are the thickness of the sample and linear absorption coefficient, respectively; I_0 is the intensity at the focal point; z_0 and z are the diffraction length of Gaussian beam and the propagation distance, respectively. By fitting the *Z*-scan data, the estimated β fall in ranges of (-7.0×10^3)~(-9.0×10^3)

cm/GW and (-1.3×10^4)~(-2.2×10^4) cm/GW in varied input powers for 2*D* Bi_2Te_3 and MoS_2/Bi_2Te_3 heterostructures, respectively (Fig. 3g). The much larger β in MoS_2/Bi_2Te_3 heterostructures suggested that the construction of MoS_2/Bi_2Te_3 heterostructures could improve the main limitation of saturation absorption intensity for 2*D* Bi_2Te_3 and the obtained MoS_2/Bi_2Te_3 heterostructures demonstrated excellent NLO saturable performance.

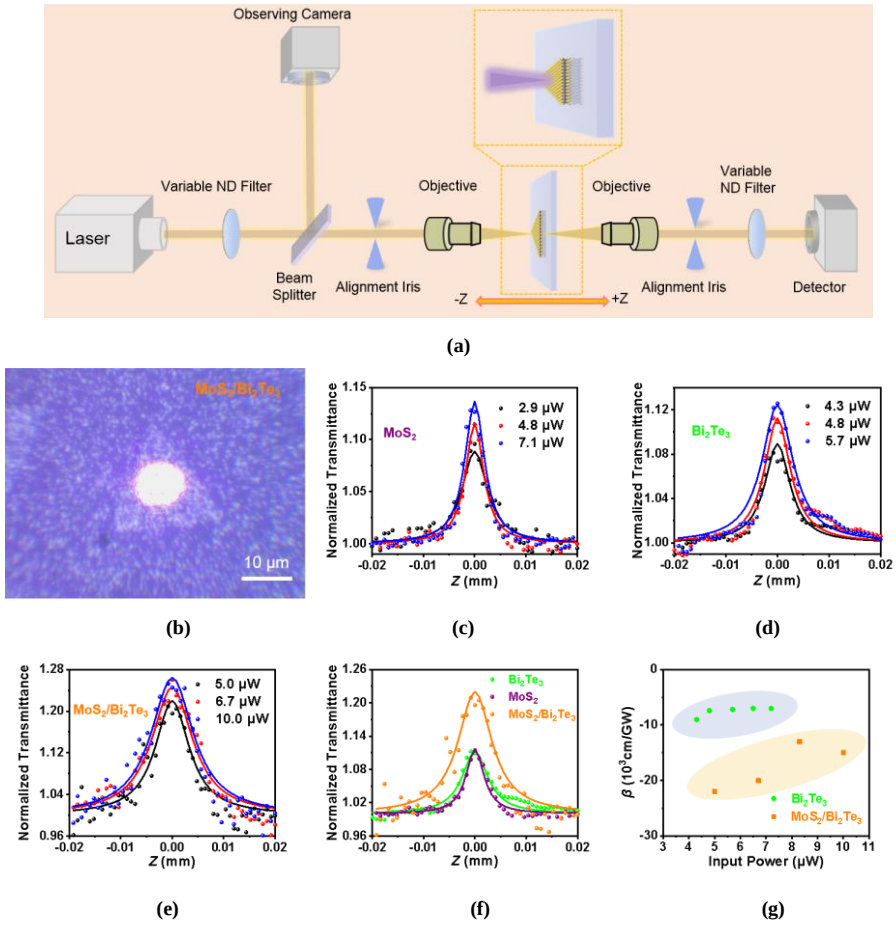

Fig. 3. (a) Schematic diagram of *Z*-scan system with optical imaging identification, (b) Optical image of a MoS_2/Bi_2Te_3 heterostructure with the laser spot irradiating, (c)~(e)Typical open aperture *Z*-scan curves of the monolayer MoS_2, Bi_2Te_3 and MoS_2/Bi_2Te_3 heterostructures at 400 nm photoexcitation with different input powers, (f) Open aperture *Z*-scan curves of Bi_2Te_3, MoS_2 and MoS_2/Bi_2Te_3 heterostructures at the same input power of 5 μW and 400 nm photoexcitation, (g) The input power dependent nonlinear absorption coefficient (β) for the Bi_2Te_3 flakes and MoS_2/Bi_2Te_3 heterostructures

3. 3 Transient optical response of the obtained MoS_2/Bi_2Te_3 heterostructures

To further explore the NLO behavior and unravel the transient optical response of the as-prepared 1L MoS_2 flakes and their MoS_2/Bi_2Te_3 heterostructures, we performed femtosecond pump-probe spectroscopic technique to investigate the ultrafast carrier dynamics under pulse irradiation at 400 nm. Similar to micro-*Z*-scan measurement, the optical microscope system was also used for facilitating the change characterizations of the carrier dynamic for the same samples in pump-probe measurement (Figs. 4a and 4b). All the measurements in MoS_2 monolayers and their MoS_2/Bi_2Te_3 heterostructures displayed two distinct photobleaching features (negative absorption bands) derived from Pauli blocking, also indicative of their saturable absorption over the entire spectral range from 550 to 800 nm (Figs. 4c and 4d). The negative absorption appearing at ~620 (~2.0 eV) and ~680 nm (~1.8 eV) corresponded to the B- and A-exciton, respectively, in agreement with the previous observations[5, 36]. And transient dynamics of photoexcited MoS_2 monolayers were mainly monitored at both A- and B-excitonic bleach positions, as shown in Fig. 4e. This bleach kinetics can be fitted on the basis of the three-exponential equation (2)[38, 41]:

$$\Delta A(t,\omega) = a(\omega)\cdot e^{-t/\tau_1} + b(\omega)\cdot e^{-t/\tau_2} + c(\omega)\cdot e^{-t/\tau_3} \quad (2)$$

where τ_1, τ_2 and τ_3 represent the carrier lifetime of the different response processes. The fast recovery time τ_1 could be mainly attributed to the exciton formation process for MoS_2 monolayers in picoseconds or subpicoseconds reported previously[35]. The second τ_2 generally corresponded to the Auger recombination or exciton-exciton annihilation in the systems[42]. τ_3 represented the typical inter-band relaxation time causing the slow-state relaxation in several hundred picoseconds[43]. We primarily compared the recovery time within the shorter time scale (τ_1) for 1L MoS_2 in the absence and presence of 2*D* Bi_2Te_3 flakes. In the absence of Bi_2Te_3, the ~620 and ~680 nm bleaches in pure 1L MoS_2 recovered within ~860 and ~620 fs, respectively. For annealed MoS_2/Bi_2Te_3 heterostructure with strong coupling between the layers, the ~620 and ~680 nm bleaches exhibited faster recovery time of ~620 and ~440 fs (Fig. 4f), respectively, which made it more feasible for varied applications such as ultrafast pulse laser generation with narrow pulse width. By contrary, the MoS_2/Bi_2Te_3 heterostructure without annealing showed slower recovery time of ~1000 and ~950 fs in the ~620 and ~680 nm bleaches, respectively (Supplementary materials, Fig. S3). Combining these results and previous work[25, 28], we proposed that the reduced carrier lifetime could also be ascribed to the electron transfer from the 1L MoS_2 to 2*D* Bi_2Te_3 besides forming excitons, consistent with the results of micro-*Z*-scan.

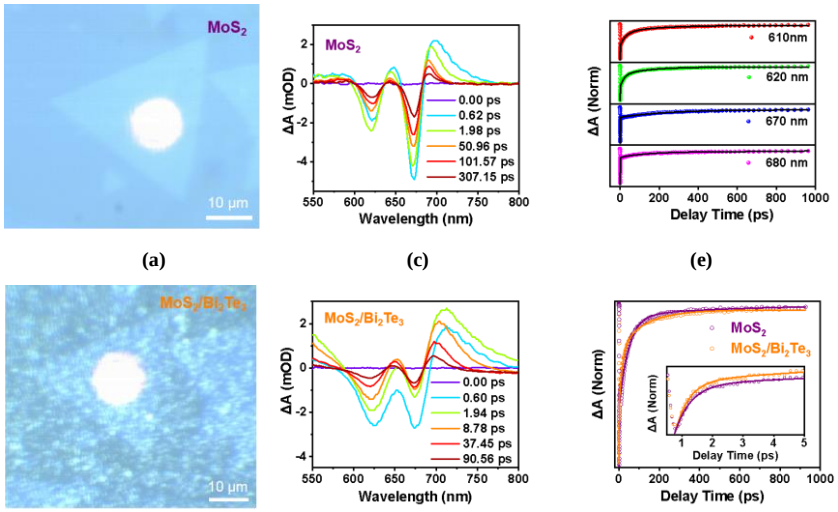

Fig. 4. (a, b) Optical images of a MoS_2 monolayer and the constructed MoS_2/Bi_2Te_3 heterostructure with the laser spot, (c, d) Representative transient absorption spectra of monolayer MoS_2 and the MoS_2/Bi_2Te_3 heterostructure at 400 nm photoexcitation, (e) Transient absorption kinetics of the MoS_2/Bi_2Te_3 heterostructure, (f) Comparison of transient absorption kinetics for the MoS_2 monolayer and its built MoS_2/Bi_2Te_3 heterostructure at ~620 nm. Inset: the enlarged decay curve recorded up to 5 ps. Solid lines in (e and f) represented the exponential fitting

Based on the unique micro-imaging pump-probe technique and successful synthesis of single crystal CVD-grown MoS_2 flakes with varied layers, we further investigated the layer-dependent ultrafast carrier dynamics of 1L, 2L, 3L and 4L MoS_2 flakes and their MoS_2/Bi_2Te_3 heterostructures in details (Fig. 5a). As shown in Fig. 5b, both the A- and B-exciton bleaching peaks redshifted with the increase of layer numbers for pure MoS_2 flakes due to the gradually decreased bandgap evolution[44]. The similar phenomena occurred in MoS_2/Bi_2Te_3 heterostructures (Fig. 5c and Supplementary materials, Figs. S4 and S5). Moreover, since the defect-assisted recombination at the surface became significant as the thickness was decreased, we observed that defect states-more 1L MoS_2 flakes demonstrated dramatically reduced carrier lifetimes than the defect states-less few-layer ones (Fig. 5d and Supplementary materials and Fig. S6), showing exactly the same trend as in the mechanically exfoliated MoS_2 flakes[45, 46]. In addition, similar to 1L MoS_2/Bi_2Te_3, the heterostructures based on few-layer MoS_2 and 2*D* Bi_2Te_3 also possessed shorter carrier recovery time (Fig. 5d).

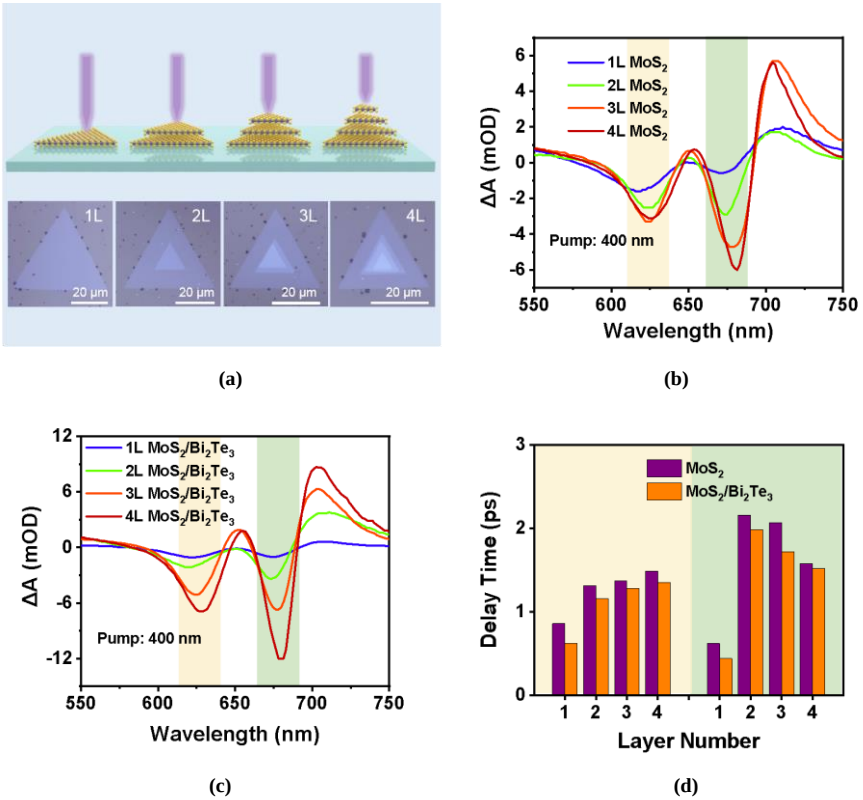

Fig. 5. (a) Schematic diagram and optical images of 1L∼4L MoS_2 flakes, (b) Time-resolved transient absorption spectra probed at 1ps for 1L∼4L MoS_2 flakes of (a), (c) Heterostructures based on another 1L∼4L MoS_2 flakes of Fig S5, (d) Statistics of the fast recovery time constant τ_1 for 1L∼4L MoS_2 (purple) and 1L∼4L MoS_2/Bi_2Te_3 heterostructures (orange), the yellow-colored left region and green-colored right region corresponded to the τ_1 values extracted from B- and A-exciton bleaching peaks

4 CONCLUSION

In summary, we have successfully constructed high-performance MoS_2/Bi_2Te_3 heterostructures by drop-casting Bi_2Te_3 flakes on CVD-grown MoS_2 flakes. The obtained heterostructures maintained good crystallinity. Owing to our homemade open aperture *Z*-scan measurements with optical imaging, the 1L MoS_2/Bi_2Te_3 heterostructures were precisely determined to possess the enhanced saturable absorption and nonlinear absorption coefficient than 2*D* Bi_2Te_3. Furthermore, layer-dependent femtosecond transient absorption spectroscopy in CVD-grown MoS_2 unveiled the shortest carrier lifetime in 1L MoS_2 than 2L, 3L and 4L MoS_2. Based on these 1L MoS_2 flakes, 1L MoS_2/Bi_2Te_3 heterostructures exhibited faster carrier lifetime of ~440 fs due to the charge transfer from the 1L MoS_2 to 2*D* Bi_2Te_3. Our work provides a novel nonlinear material with superior saturable absorption properties and provides novel insight for the design of high-performance nonlinear materials by effectively combining the optical advantages of different 2*D* materials.

REFERENCES

(1) You, J. W.; Bongu, S. R.; Bao, Q.; Panoiu, N. C. Nonlinear optical properties and applications of 2*D* materials: theoretical and experimental aspects. *Nanophotonics* **2019**, 8, 63–97.

(2) Liu, X. F.; Guo, Q. B.; Qiu, J. R. Emerging low-dimensional materials for nonlinear optics and ultrafast photonics. *Adv. Mater.* **2017**, 29, 1605886–29.

(3) Splendiani, A.; Sun, L.; Zhang, Y. B.; Li, T. S.; Kim, J.; Chim, C. Y.; Galli, G.; Wang, F. Emerging photoluminescence in monolayer MoS_2. *Nano Lett.* **2010**, 10, 1271–1275.

(4) Lee, H. S.; Min, S. W.; Chang, Y. G.; Park, M. K.; Nam, T.; Kim, H.; Kim, J. H.; Ryu, S.; Im, S. MoS_2 nanosheet phototransistors with thickness-modulated optical energy gap. *Nano Lett.* **2012**, 12, 3695–3700.

(5) Wang, K. P.; Wang, J.; Fan, J. T.; Lotya, M.; Neill, A. O.; Fox, D.; Feng, Y. Y.; Zhang, X. Y.; Jiang, B. X.; Zhao, Q. Z.; Zhang, H. Z.; Coleman, J. N.; Zhang, L.; Blau, W. J. Ultrafast saturable absorption of two-dimensional MoS_2 nanosheets. *ACS Nano* **2013**, 7, 9260–9267.

(6) Feng, C.; Zhang, X. Y.; Wang, J.; Liu, Z. J.; Cong, Z. H.; Rao, H.; Wang, Q. P.; Fang, J. X. Passively mode-locked Nd^{3+}:YVO_4 laser using a molybdenum disulfide as saturable absorber. *Opt. Mater. Express* **2016**, 6, 1358−1366.

(7) Wang, K.; Yang, K.; Zhang, X.; Zhao, S.; Luan, C.; Liu, C.; Wang, J.; Xu, X.; Xu, J. Passively Q-switched laser at 1.3 μm with few-layered MoS_2 saturable absorber. *IEEE J. Sel. Top. Quantum Electron.* **2017**, 23, 71−75.

(8) Bayesteh, S.; Mortazavi, S. Z.; Reyhani, A. Role of precursors' ratio for growth of two-dimensional MoS_2 structure and investigation on it s nonlinear optical properties. *Thin Solid Films* **2018**, 663, 37−43.

(9) Tsai, D. S.; Liu, K. K.; Lien, D. H.; Tsai, M. L.; Kang, C. F.; Lin, C. A.; Li, L. J.; He, J. H. Few-layer MoS_2 with high broadband photogain and fast optical switching for use in harsh environments. *ACS Nano* **2013**, 7, 3905−3911.

(10) Wu, K.; Chen, B. H.; Zhang, X. Y.; Zhang, S. F.; Guo, C. S.; Li, C.; Xiao, P. S.; Wang, J.; Zhou, L. J.; Zou, W. W.; Chen, J. P. High-performance mode-locked and Q-switched fiber lasers based on novel 2*D* materials of topological insulators, transition metal dichalcogenides and black phosphorus: review and perspective (invited). *Opt. Commun.* **2018**, 406, 214−229.

(11) Shi, H.; Yan, R.; Bertolazzi, S.; Brivio, J.; Gao, B.; Kis, A.; Jena, D.; Xing, H. G.; Huang, L. Exciton dynamics in suspended monolayer and few-layer MoS_2 2*D* crystals. *ACS Nano* **2013**, 7, 1072−1080.

(12) Cunningham, P. D.; McCreary, K. M.; Hanbicki, A. T.; Currie, M.; Jonker, B. T.; Hayden, L. M. Charge trapping and exciton dynamics in large-area CVD grown MoS_2. *J. Phys. Chem. C* **2016**, 120, 5819−5826.

(13) Wang, Q.; Ge, S.; Li, X.; Qiu, J.; Ji, Y.; Feng, J.; Sun, D. Valley carrier dynamics in monolayer molybdenum disulphide from helicity resolved ultrafast pump-probe spectroscopy. *ACS Nano* **2013**, 7, 11087−11093.

(14) Wang, S.; Yu, H.; Zhang, H.; Wang, A.; Zhao, M.; Chen, Y.; Mei, L.; Wang, J. Broadband few-layer MoS_2 saturable absorbers. *Adv. Mater.* **2014**, 26, 3538−3544.

(15) Zhang, H.; Liu, C. X.; Qi, X. L.; Dai, X.; Fang, Z.; Zhang, S. C. Topological insulators in Bi_2Se_3, Bi_2Te_3 and Sb_2Te_3 with a single Dirac cone on the surface. *Nat. Phys.* **2009**, 5, 438−442.

(16) Zhao, C.; Zhang, H.; Qi, X.; Chen, Y.; Wang, Z.; Wen, S.; Tang, D. Ultra-short pulse generation by a topological insulator based saturable absorber. *Appl. Phys. Lett.* **2012**, 101, 211106−4.

(17) He, X.; Zhang, H.; Lin, W.; Wei, R.; Qiu, J.; Zhang, M.; Hu, B. PVP-Assisted solvothermal synthesis of high-yielded Bi_2Te_3 hexagonal nanoplates: application in passively Q-switched fiber laser. *Sci. Rep.* **2015**, 5, 15868−10.

(18) Wang, Y. R.; Lee, P.; Zhang, B. T.; Sang, Y. H.; He, J. L.; Liu, H.; Lee, C. K. Optical nonlinearity engineering of a bismuth telluride saturable absorber and application of a pulsed solid state laser therein. *Nanoscale* **2017**, 9, 19100−19107.

(19) Yang, J.; Tian, K.; Li, Y.; Dou, X.; Ma, Y.; Han, W.; Xu, H.; Liu, J. Few-layer Bi_2Te_3: an effective 2*D* saturable absorber for passive Q-switching of compact solid-state lasers in the 1-μm region. *Opt. Express* **2018**, 26, 21379−21389.

(20) Yin, K.; Zhang, B.; Li, L.; Jiang, T.; Zhou, X.; Hou, J. Soliton mode-locked fiber laser based on topological insulator Bi_2Te_3 nanosheets at 2 μm. *Photonics Res.* **2015**, 3, 72−76.

(21) Geim, A. K.; Grigorieva, I. V. Van der Waals heterostructures. *Nature* **2013**, 499, 419−425.

(22) Neupane, G. P.; Zhou, K.; Chen, S.; Yildirim, T.; Zhang, P.; Lu, Y. In-plane isotropic/anisotropic 2*D* van der Waals heterostructures for future devices. *Small* **2019**, 15, 1804733−16.

(23) Zheng, W.; Zheng, B.; Yan, C.; Liu, Y.; Sun, X.; Qi, Z.; Yang, T.; Jiang, Y.; Huang, W.; Fan, P.; Jiang, F.; Ji, W.; Wang, X.; Pan, A. Direct vapor growth of 2*D* vertical heterostructures with tunable band alignments and interfacial charge transfer behaviors. *Adv. Sci.* **2019**, 6, 1802204−9.

(24) Hong, X.; Kim, J.; Shi, S. F.; Zhang, Y.; Jin, C.; Sun, Y.; Tongay, S.; Wu, J.; Zhang, Y.; Wang, F. Ultrafast charge transfer in atomically thin MoS_2/WS_2 heterostructures. *Nat. Nanotechnol.* **2014**, 9, 682−686.

(25) Bellus, M. Z.; Li, M.; Lane, S. D.; Ceballos, F.; Cui, Q.; Zeng, X. C.; Zhao, H. Type-I van der Waals heterostructure formed by MoS_2 and ReS_2 monolayers. *Nanoscale Horiz.* **2017**, 2, 31−36.

(26) Sun, X.; Zhang, B.; Li, Y.; Luo, X.; Li, G.; Chen, Y.; Zhang, C.; He, J. Tunable ultrafast nonlinear optical properties of graphene/MoS_2 van der Waals heterostructures and their application in solid-state bulk lasers. *ACS Nano* **2018**, 12, 11376−11385.

(27) Luo, S.; Qi, X.; Li, J.; Ren, L.; Guo, G.; Peng, Q.; Li, J.; Zhong, J. Significant photoluminescence quenching and charge transfer in the MoS_2/Bi_2Te_3 heterostructure. *J. Phys. Chem. Solids* **2019**, 12, 337−342.

(28) Sung, J. H.; Cha, S.; Heo, H.; Sim, S.; Kim, J.; Choi, H.; Jo, M. H. Ultrafast hot-carrier photovoltaics of type-I monolayer heterojunctions in the broad spectral ranges. *ACS Photonics* **2017**, 4, 429−434.

(29) Zheng, J.; Yan, X.; Lu, Z.; Qiu, H.; Xu, G.; Zhou, X.; Wang, P.; Pan, X.; Liu, K.; Jiao, L. High-mobility multilayered MoS_2 flakes with low contact resistance grown by chemical vapor deposition. *Adv. Mater.* **2017**, 29, 1604540–6.

(30) Song, J.; Xia, F.; Zhao, M.; Zhong, Y. L.; Li, W.; Loh, K. P.; Caruso, R. A.; Bao, Q. Solvothermal growth of bismuth chalcogenide nanoplatelets by the oriented attachment mechanism: an in situ PXRD study. *Chem. Mater.* **2015**, 27, 3471–3482.

(31) Jiao, L. Y.; Fan, B.; Xian, X. J.; Wu, Z. Y.; Zhang, J.; Liu, Z. F. Creation of nanostructures with poly(methyl methacrylate)-mediated nanotransfer printing. *J. Am. Chem. Soc.* **2008**, 130, 12612–12613.

(32) Liang, Y.; Wang, W.; Zeng, B.; Zhang, G.; Huang, J.; Li, J.; Li, T.; Song, Y.; Zhang, X. Raman scattering investigation of Bi_2Te_3 hexagonal nanoplates prepared by a solvothermal process in the absence of NaOH. *J. Alloys Compd.* **2011**, 509, 5147–5151.

(33) Qi, X.; Ma, W.; Zhang, X.; Zhang, C. Raman characterization and transport properties of morphology-dependent two-dimensional Bi_2Te_3 nanofilms. *Appl. Surf. Sci.* **2018**, 457, 41–48.

(34) Lee, C.; Yan, H.; Brus, L. E.; Heinz, T. F.; Hone, J.; Ryu, S. Anomalous lattice vibrations of single-and few-layer MoS_2. *ACS Nano* **2010**, 4, 2695–2700.

(35) Aleithan, S. H.; Livshits, M. Y.; Khadka, S.; Rack, J. J.; Kordesch, M. E.; Stinaff, E. Broadband femtosecond transient absorption spectroscopy for a CVD MoS_2 monolayer. *Phys. Rev. B* **2016**, 94, 035445–7.

(36) Pogna, E. A.; Marsili, M.; De Fazio, D.; Dal Conte, S.; Manzoni, C.; Sangalli, D.; Yoon, D.; Lombardo, A.; Ferrari, A. C.; Marini, A.; Cerullo, G.; Prezzi, D. Photo-induced bandgap renormalization governs the ultrafast response of single-layer MoS_2. *ACS Nano* **2016**, 10, 1182–1188.

(37) Britnell, L.; Ribeiro, R. M.; Eckmann, A.; Jalil, R.; Belle, B. D.; Mishchenko, A.; Kim, Y. J.; Gorbachev, R. V.; Georgiou, T.; Morozov, S. V.; Grigorenko, A. N.; Geim, A. K.; Casiraghi, C.; Castro Neto, A. H.; Novoselov, K. S. Strong light-matter interactions in heterostructures of atomically thin films. *Science* **2013**, 340, 1311–1314.

(38) Jiang, Y.; Miao, L.; Jiang, G.; Chen, Y.; Qi, X.; Jiang, X. F.; Zhang, H.; Wen, S. Broadband and enhanced nonlinear optical response of MoS_2/graphene nanocomposites for ultrafast photonics applications. *Sci. Rep*. **2015**, 5, 1–12.

(39) Mu, H.; Wang, Z.; Yuan, J.; Xiao, S.; Chen, C.; Chen, Y.; Chen, Y.; Song, J.; Wang, Y.; Xue, Y.; Zhang, H.; Bao, Q. Graphene-Bi_2Te_3 heterostructure as saturable absorber for short pulse generation. *ACS Photonics* **2015**, 2, 832–841.

(40) Zhang, H.; Lu, S. B.; Zheng, J.; Du, J.; Wen, S. C.; Tang, D. Y.; Loh, K. P. Molybdenum disulfide (MoS_2) as a broadband saturable absorber for ultra-fast photonics. *Opt. Express* **2014**, 22, 7249–7260.

(41) Ye, Y.; Xian, Y.; Cai, J.; Lu, K.; Liu, Z.; Shi, T.; Du, J.; Leng, Y.; Wei, R.; Wang, W.; Liu, X.; Bi, G.; Qiu, J. Linear and nonlinear optical properties of few-layer exfoliated SnSe nanosheets. *Adv. Opt. Mater.* **2019**, **7**, 1800579–8.

(42) Ceballos, F.; Cui, Q.; Bellus, M. Z.; Zhao, H. Exciton formation in monolayer transition metal dichalcogenides. *Nanoscale* **2016**, 8, 11681–11688.

(43) Kime, G.; Leontiadou, M. A.; Brent, J. R.; Savjani, N.; O'Brien, P.; Binks, D. Ultrafast charge dynamics in dispersions of monolayer MoS_2 nanosheets. *J. Phys. Chem. C* **2017**, 121, 22415–22421.

(44) Mak, K. F.; Lee, C.; Hone, J.; Shan, J.; Heinz, T. F. Atomically thin MoS_2: a new direct-gap semiconductor. *Phys. Rev. Lett*. **2010**, 105, 136805–4.

(45) Wang, Y. Z.; Guo, Z. Y.; You, J.; Zhang, Z.; Zheng, X.; Cheng, X. G. Ultrafast nonlinear optical excitation behaviors of mono- and few-layer two dimensional MoS_2. *Photonic Sens.* **2019**, 9, 1–10.

(46) Wang, H. N.; Zhang, C. J.; Rana, F. Surface recombination limited lifetimes of photoexcited carriers in few-layer transition metal dichalcogenide MoS_2. *Nano Lett*. **2015**, 15, 8204–8210.